Supporting Information

Shemesh et al. 10.1073/pnas.1419997111

SI Text

Theory: Detailed Derivation of the Morphology Model

Geometrical Representation of ER Tubules and Sheets. We consider all ER morphologies as composed of sheets and tubules. ER sheets are made up of two apposing planar membranes and edge surfaces that connect these two membranes. The edge surfaces are either located at the sheet periphery or form internal edges within sheets. We therefore describe a sheet by two components:

i) The planar part of the sheet consisting of two parallel membrane surfaces, separated by a distance *d* (Fig. 1*B*). We represent this part as a single surface of zero thickness, lying in between the two membranes. This surface is referred to as the sheet plane.

ii) The membrane of the sheet edge, the shape of which can be approximated by a hemicylinder with an axis bending in the sheet plane. The diameter of the cylindrical edge is equal to the distance, *d*, between the sheet membranes (Fig. 1*B*). We represent the edge of the sheet as a curved line that coincides with the axis of the hemicylinder. This line forms the boundary of the sheet plane and is referred to as the edge line.

Tubules are considered to be complete cylinders and, analogously to the sheet edges, are represented in our model by lines running through their axes (Fig. 1*A*). Tubules can connect with the sheet edge; in our model, this is represented as the branching of the edge line into a tubule line.

Different ER Morphologies. We relate each morphological state of the ER to specific shapes adopted by sheets and tubules:

i) Tubular network: tubules connected by small triangular sheets with concave edges, called three-way junctions.

ii) Network with interspersed sheets: large flat sheets that are each connected to multiple long tubules.

iii) Fenestrated state: sheets connected by short tubules, such that the mean length of tubules is smaller than the distance between tubule connections on a sheet.

iv) Sheet stacks: parallel sheets that are connected by helicoidal connections. These intersheet connectors consist of sheet surfaces that are shaped as hollow helicoids, and contain internal edge lines of helical shape (1).

We refer to the first three morphologies as network states, and the fourth morphology as a helicoidal state.

Energy of ER Structural Elements and Configurations. Our hypothesis is that each geometrical state of the ER corresponds to a minimum of the overall energy of the system. As contributions to this energy, we consider the elastic energies of the sheet planes and edge lines, as well as entropic contributions related to the protein composition of sheet edges and tubules. Specifically, the following energy terms were used:

1. The elastic bending energy of the sheet plane. This energy, related to a unit area of the sheet plane, f_s, is given by the Helfrich equation (2):

$$f_s = \frac{1}{2}\kappa J^2, \qquad \textbf{[S2]}$$

where J is the total curvature (3) and κ is the bending modulus of the sheet plane. The reference state for a sheet is therefore a flat, edgeless surface. The bending modulus κ is taken to be 40 $k_B T$, which is the value characterizing a single lipid bilayer (4) multiplied by a factor of 2 to account for contributions of the two sheet membranes. Eq. **S1** describes the energy associated with bending the initially flat sheet plane into a shape with total curvature *J.* The bending energy of the sheet plane, F_s, is obtained by integration of Eq. **S1** over the sheet plane area,

$$F_S = \iint f_s dA. \qquad \textbf{[S2]}$$

2. The total elastic energy of the sheet edge can be seen as consisting of two contributions; one is related to the curvature of the edge membrane in the cross-section normal to the sheet surface (this is the curvature of the hemicylindrical edge in a cross-section perpendicular to the cylinder axis). We assume that this curvature is generated by two types of curvature-stabilizing proteins, R and S, which localize to the sheet edges. This curvature and the related energy do not depend on the shape of the edge line. The second contribution to the elastic energy of the edges is related to the bending of the edge line. Using the expressions for the area and mean curvature of a toroidal surface element, we find that the bending energy, per unit length of the edge line, of a curved hemicylindrical surface is given by

$$f_e = \frac{\kappa}{2}\int\limits_{\alpha-\frac{\pi}{2}}^{\alpha+\frac{\pi}{2}} \frac{4\cdot(1+d\cdot c\cdot\cos(\theta))^2}{(1+d\cdot c\cdot\cos(\theta))\cdot d}d\theta, \qquad \textbf{[S3]}$$

where d is the sheet thickness, θ is the angle between the sheet plane and the normal of a point on the hemicylindrical edge surface (Fig. S1), c is the space curvature of the edge line, and α is the angle between the normal to the osculating plane of the curve and the normal of the sheet surface (Fig. S1). From the numerical evaluation of the integral in Eq. **S3**, we find that the minimal bending energy of the edge occurs if $\alpha = 0$, i.e., for edge lines that curve in the sheet plane. For such edge lines, the elastic bending energy of the sheet edge per unit length of the edge line, f_e, is approximated by

$$f_e = \frac{1}{2}k_e\left(\zeta^2 - 2\zeta\zeta^*\right), \qquad \textbf{[S4]}$$

where k_e is the edge line bending modulus, $\zeta = c\cdot\cos\alpha$ is the geodesic curvature of the edge line, and ζ^* is the spontaneous curvature of the edge line. Eq. **S4** gives the energy required to bend the edge line away from its preferred shape. The reference (zero-energy) state of the edge is that of vanishing geodesic curvature, $\zeta = 0$. We assume that both types of curvature-stabilizing proteins, R and S, generate positive cross-sectional curvature of the sheet edge. However, they would favor different spontaneous curvatures of the edge line, ζ^*. The R and S proteins would generate edge-lines with preferred curvatures ζ_R, and ζ_S, referred to as the spontaneous line curvatures generated by R and S proteins, respectively. We assume that the overall local spontaneous curvature of the edge, ζ^*, equals the weighted average of the spontaneous line curvatures of the constituent curvature-stabilizing proteins, $\zeta^* = \zeta_R + (\zeta_S - \zeta_R)\varphi$, where φ is the local fraction of S-protein molecules relative to the total protein number, φ = [S]/([S] + [R]). In our computations, we assume

$\zeta_R = 0$, meaning that R proteins favor a straight edge line, whereas the S proteins having $\zeta_S < 0$ would generate a negative curvature of the edge. The total bending energy of the edge line, F_e, is obtained by integration of Eq. **S4** over the length L_{tot} of the edge line,

$$F_e = \oint f_e dL. \qquad \textbf{[S5]}$$

A mathematically analogous treatment to our model of the sheet edge was used for computing the shapes of closed 2D membrane surfaces, characterized by a bending elasticity and composed of several kinds of elastic elements (5).

3. The elastic energy associated with the Gaussian curvature of the system. This energy, related to a unit area of the membrane surface, is given by (2)

$$f_G = \bar{\kappa} K, \qquad \textbf{[S6]}$$

where K is the Gaussian curvature and $\bar{\kappa}$ is the modulus of Gaussian curvature of the membrane. Though the exact value of $\bar{\kappa}$ is unknown and can depend on the lipid and protein composition of the membrane, we consider it to lie in the range of values reported in the literature, $\bar{\kappa} = -0.3\kappa \ldots -0.8\kappa$ (6, 7). The energy term (6) is relevant only when the membrane undergoes changes in topology, such as the generation of fenestrations, junctions, or helicoids.

4. The energy F_γ is associated with the effective line tension of the sheet edge, γ_e. The line tension γ_e accounts for all of the energy costs, per unit length of edge line, that are associated with splitting a tubule into a hemicylindrical edge surface connected with two planar membrane surfaces. Assuming that γ_e does not vary along the edge, the energy F_γ is given by

$$F_\tau = \gamma_e L_e, \qquad \textbf{[S7]}$$

where L_e is the length of the sheet edges (excluding tubules). In our model, we estimate the entropic contribution to the line tension, γ_e, which results from the fact that arcs formed by the curvature-stabilizing proteins can adopt many more positions on a tubule compared with a sheet edge, because they have twice the surface area available (cylinder vs. hemicylinder). Accordingly, the line tension can be expressed by

$$\gamma_e = \frac{k_B T}{l_e} \ln(2), \qquad \textbf{[S8]}$$

where k_B is the Boltzmann constant, T is the absolute temperature, and l_e is the average distance between arcs of curvature-stabilizing proteins along tubules or the edge line (Fig. 1*C*). Based on previous considerations, l_e was taken to be 45 nm. Other possible contributions to the line tension, such as the elastic bending energy that arises from the imperfect match between the curvature of the edge surfaces and that of the planar surfaces, are not included in our calculations.

5. The entropic energy associated with the uneven distribution of the two types of curvature-stabilizing proteins, R and S, along the edge line. This energy term resists the partitioning of the two types of curvature-stabilizing proteins into separate domains along the edge line. This contribution to the system energy, per unit length of the edge line, is given by

$$f_m = \frac{k_B T}{l_e} [\varphi \ln(\varphi) + (1-\varphi)\ln(1-\varphi)]. \qquad \textbf{[S9]}$$

It should be noted that φ can vary along the edge line. The total entropic energy of mixing, F_m, is obtained by integration of Eq. **S9** over the entire length L_{tot} of the edge line, including the length of tubules. The mean of φ over L_{tot} is equal to the global fraction of S-type proteins, Φ.

Though not included in our model, yet another entropic term may contribute to the energy of a network. This term results from the number of configurations that are available to the system in each morphology (8). This contribution would tend to disfavor sheets with multiple connections, and would promote disassembly of the network into individual short tubules. This entropic term is expected to be most relevant for dilute systems (9), i.e., systems with few connectors.

Finding the Optimal Morphology. In the case where the thickness of a curvature-stabilizing arc, l_p, is much smaller than the distance between arcs along the edge line, l_e, the total length of edges in the system, L_{tot} is given by

$$L_{tot} = C_{tot} \frac{2A_{mem}}{\pi d l_p} l_e, \qquad \textbf{[S10]}$$

where A_{mem} is the total membrane area. L_{tot} is divided between the total length of tubules, L_t, and the total length of sheet edges, L_e, such that $L_{tot} = L_e + 2L_t$. Based on previous estimates, we use $l_e = 45$ nm and $l_p = 4$ nm (10).

We assume that helicoidal states do not coexist with network states, and further that sheets in mixed sheet–tubule morphology remain flat. Thus, the contribution of the Gaussian elastic energy (6) for the sheet-tubule states may be written as

$$\iint f_G dA = \bar{\kappa} 4\pi N_s \left(1 - \frac{n}{2}\right), \qquad \textbf{[S11]}$$

where N_s is the number of sheets in the system, and n is the number of tubule connections per sheet. For the helicoidal states, the Gaussian energy term (6) can be written as

$$\iint f_G dA = \bar{\kappa} 4\pi \left(N_s + \frac{m}{2} - N_s m\right), \qquad \textbf{[S12]}$$

where m is the number of helicoids per sheet.

Theory: Computational Procedures

The total energy of the system was numerically minimized using Surface Evolver, a finite element solver package (11), and MatLab code. The total membrane surface and the number of curvature-stabilizing proteins R and S were kept constant for each minimization. The minimization procedure for the network morphologies optimizes the following variables:

- Number of sheets in the system, N_s.
- Number of tubules per sheet, n.
- Shape of the sheet edges.
- Local distribution of S and R type proteins along edges and tubules, φ.

For helicoidal states, we calculate the optimal values of

- Number of sheets N_s.
- Helicoid parameters: internal radius, external radius, and pitch.
- Local distribution of S and R type proteins along the inner and outer edges.

We determine the optimal values of the variables that describe each morphology, as a function of the system variables $\{C_{tot}, \Phi\}$. The calculations were performed with $\zeta_S = -10\ \mu\text{m}^{-1}$ and $\bar{\kappa} = -20\ k_B T$. The total membrane area of the system was kept fixed at 500 μm^2. We have repeated calculations for different spontaneous curvatures ζ_S with absolute values in the range of 5 to 30 μm^{-1} and for different values of the modulus of Gaussian curvature, $\bar{\kappa}$, varying in the range of −10 to −40 k_BT. No qualitative differences in the modeling results were obtained. At parameter values that result in a small optimal number of larger sheets ($N_s < 100$), each with multiple tubule connections ($n > 6$), the minimization procedure could not robustly converge on the optimal connectivity, n, due to small relative variations in the energy landscape of the parameter space.

Numerical calculations were performed by a combination of MatLab code and Surface Evolver script. For a detailed description of the algorithms and convergence criteria, see ref. 11. The Surface Evolver script is divided into three modules, described below. The modules were executed in a MatLab shell for determining the global minimum of the parameter space.

Module A. Calculates the energy associated with the shape of the sheet–junction and associated tubules. The local distribution of spontaneous curvature along the sheet and tubule edges is determined in module B.

Input parameters: n (sheet symmetry), A (sheet area), $Lmax$ (maximal edge per sheet)

- Local spontaneous curvature along the boundary edges.

Fixed parameters: $\kappa, \kappa_e, \gamma_e, \bar{\kappa}$
Energy methods:

- Surface-bending energy: *star_perp_sq_mean_curvature.* Defined over boundary edges (calculates surface curvature). Modulus = $\kappa/2$.
- Edge-bending energy 1: *sqcurve_string_marked* (parameter_1 = 2). Defined over boundary vertices. Modulus = $\kappa_e/2$.
- Edge bending energy 2: *vertex_scalar_integral*, sc_local × orientation_local × *sqcurve_string_marked* (parameter_1 = 1). Defined over boundary vertices. Modulus = κ_e.
- Line tension: *edge_length.* Defined over boundary edges of sheets only. Modulus = γ_e.
- Gaussian contribution: (scalar parameter) − (pi − (2 × pi/n)) × $\bar{\kappa}$
- Hookean energy (applied to some edges to assist in convergence, not included in the total shape energy): *hooke_energy.* Defined on edges near constraints.

Constraints:

- Reflective constraint: $x = 0$
- Reflective constraint: $y = x/\tan(2\pi n)$
- Fixed constraint: *facet_area=A/n*
- Nonnegative constraint: *edge_length* < *Lmax/n*

Custom vertex properties:

- *orientation_local* = custom vertex attribute to sign the orientation of each segment (1 clockwise, −1 counterclockwise).
- *cs_local* = custom vertex property to designate the effective spontaneous curvature at each vertex.

Outputs:

- Total energy
- Vertex positions
- Edge length
- Curvatures at vertices

Module B. Calculates the optimal distribution along a fixed shape. The concentrations of S-type proteins along boundary edges in module A are represented by the y coordinate of vertices in module B.

Fixed parameters:

- l_e, κ_e, ζ_S, Φ

Input parameters:

- Curvature of edges from output of module A.
- Length of edges from output of module A.

Energy methods:

- Line-bending energy (term due to local spontaneous curvature): *vertex_scalar_intergral.* Modulus = $-\kappa_e$. Scalar_integrand = y × ζ_S× edgeCurvature × edgeLength.
- Entropic energy of S-type protein distribution: *vertex_scalar_integral.* Modulus = 1. Scalar_integrand = y × *log*(y) + (1− y) × *log*(1 − y)) × edgeLength/l_e.

Custom vertex properties:

- edgeLength = custom vertex attribute storing the length of the corresponding edge from module A.
- *edgeCurvature* = custom vertex attribute storing the curvature of the corresponding length from module A.

Constraints:

- Nonnegative constraint: $y > 0$.
- Nonnegative constraint: $(1 - y) > 0$.
- Fixed constraint: vertex_scalar_integral(y × edgeLength) = vertex_scalar_integral(Φ× edgeLength).

Outputs:

- Optimal spontaneous curvature for each edge element of module A.
- Entropic energy of mixing.

The optimal shape and optimal S-type protein distribution are calculated by iterating module A and module B. The initial guess morphology is taken as flat sheets with straight edges and a homogeneous distribution $y = \Phi$. Convergence of A–B iterations is defined when for each edge element i: $|y_i(step) - y_i(step - 1)| < 0.01 \cdot y_i(step)$. Based on symmetry, the total energy is multiplied by n.

Module C. Calculates the surface and edge bending energy for a helicoidal element.

Fixed parameters:

- $\kappa, \kappa_e, \zeta_S, \gamma_e, \bar{\kappa}$.

Input parameters:

- A (area per helicoid per sheet in stack), L, N (helicoids per sheet), M (sheets in stack), Φ

Optimizing parameters:

- Rin, rout, pitch

Energy methods:

- Surface-bending energy: *star_perp_sq_mean_curvature.* Defined over boundary edges (calculates surface curvature). Modulus = $\kappa/2$.
- Edge-bending energy: edge_scalar_integral. Defined over internal boundary edges. Modulus = $\kappa_e/2$. Scalar_integrand = (rin/(rin^2 + pitch^2) − Φ·ζ_S)^2.
- Gaussian energy: (scalar parameter) −2 × 2 ×π× $\bar{\kappa}$ × (N − $N/M/2$ + 1).
- Line tension: *edge_length.* Defined over boundary edges of sheets only. Modulus = γ_e.

Constraints:

- Fixed constraint: *facet_area* = A.

- Fixed constraint: 2 × pi × sqrt(rin^2 + pitch^2) = *L*.

SI Experimental Procedures

Transient Expression Experiments with COS Cells. HA-tagged wild-type human lunapark (Lunapark-HA) was TOPO cloned into pcDNA3.1d using full-length lunapark cDNA (Open Biosystems; accession no. BC105134, cDNA KIAA1715) as a template and forward and reverse primers. The reverse primer contained the nucleotide sequence of a HA tag in frame with the Kozak sequence of lunapark.

COS-7 cells were transfected with 1 μg or 2 μg of plasmid DNA using the transfection reagent Lipofectamine 2000 (Invitrogen). The cells were incubated for 12 h at 37 °C and 5% (vol/vol) CO_2 in DMEM, 10% (vol/vol) FBS, and 1 mM sodium pyruvate. For immunofluorescence experiments, the cells were trypsinized and transferred onto acid-washed glass coverslips. They were incubated for 24 h in a 12-well tissue culture dish. The cells were then fixed with PBS containing 4% (vol/vol) paraformaldehyde for 30 min at room temperature. The cells were washed with PBS and permeabilized with PBS containing 0.1% Triton X-100 (Thermo) for 10 min at room temperature.

Immunocytochemistry was carried out by incubating the permeabilized cells with antibodies against the HA-tag (rat anti-HA, 1:200, Roche) or the endogenously expressed lunapark protein (rabbit anti-Lunapark; Sigma-Aldrich), together with antibodies against the luminal ER protein calreticulin (rabbit anti-calreticulin or chicken anti-calreticulin; Abcam) or against the ER membrane proteins Rtn4a/b (goat anti-Rtn4a/b, N-18; Santa Cruz). All antibodies were diluted in PBS containing 1% calf serum. The cells were incubated with the primary antibodies for 45 min at room temperature, washed three times with PBS, and then incubated with the respective secondary antibodies for 45 min. The various secondary antibodies were diluted 1:500 in PBS, 1% calf serum (from Life Technologies: Alexa Fluor 488 goat anti-rat, Alexa Fluor 568 goat anti-rabbit, Alexa Fluor 488 donkey anti-rat, Alexa Fluor 568 donkey-anti goat, and Alexa Fluor 488 donkey anti-rabbit; from Jackson ImmunoResearch: Alexa Fluor 647 AffiniPure donkey anti-chicken). After incubation with the secondary antibodies, the cells were washed three times in PBS and mounted on glass slides using Fluoromount G as mounting solution. Images were captured using a Yokogawa spinning-disk confocal on a Nikon TE2000U inverted microscope with a 100× Plan Apo N.A. 1.4 objective lens, a Hamamatsu ORCA ER-cooled CCD camera, and MetaMorph software. For data presentation, the image depth was adjusted using Adobe Photoshop.

To quantify the phenotype caused by Lnp-HA overexpression, the transfected cells were stained with an antibody specific for lunapark and analyzed by confocal microscopy as described above. To record a representative volume of the cells to determine the mean lunapark expression level, stacks of three images were acquired with a distance of 0.25 μm between the planes of the stack. The stacks were converted into maximum-intensity projections and the mean lunapark expression level was determined relative to the endogenous level of untransfected cells. The cells were binned according to lunapark expression levels and the number of cells with different ER phenotypes was determined.

For depletion of lunapark by RNAi, COS7 cells were seeded at ~2% confluence onto acid-washed glass coverslips in a 12-well tissue culture dish. After 12 h at 37 °C and 5% (vol/vol) CO_2 in DMEM containing 10% (vol/vol) bovine serum, the cells were transfected with siRNA oligonucleotides (CACCTTTAGCAAGACCTAT) or scrambled siRNA (40 nM final concentration; Ambion Silencer Select) using the transfection reagent RNAi max (Life Technologies). The transfected cells were incubated for 72 h and then fixed as described above. To assess the degree of lunapark depletion and the associated changes in ER morphology, the cells were stained using antibodies against calreticulin (Abcam) and lunapark (Sigma-Aldrich).

To quantify the increase in ER area after lunapark depletion, stacks of three images were acquired for each marker with a distance of 0.25 μm between the stack planes. The image stacks were converted into maximum-intensity projections and the cells were segmented manually in ImageJ (National Institutes of Health). The mean lunapark fluorescence was determined for each cell and the ER area was segmented using the automated trainable WEKA segmentation plugin in ImageJ/Fiji (wiki.imagej.net/Trainable_Weka_Segmentation). The WEKA pixel classifier is based on machine-learning algorithms to classify individual pixels of the analyzed images as belonging to an object or the background. To segment the ER, the respective classifiers were trained on example images of cells treated with lunapark RNAi or scrambled control RNAi using the standard settings for the training features, including Gaussian blur, Hessian matrix, membrane projections, a Sobel filter, and difference of Gaussians. A detailed explanation of the algorithms underlying the feature training can be found at the ImageJ/Fiji website. The trained classifier was then applied to the whole dataset in batch mode and the resulting segmentations of every cell saved as binary images showing the ER and the background. These binary images were used to determine the peripheral ER area for every cell. The ratio between the ER area and total cell area was determined using the ImageJ measuring tool. For data display, the cells were binned according to their fractional ER area and the number of cells per bin was plotted in a histogram as percentage of all cells analyzed (MatLab).

Stable Expression of Lunapark in COS Cells. The lunapark coding sequence was PCR amplified from the Lnp-HA construct, fused to a C-terminal mCherry tag, and inserted into the pHAGE2 vector using PacI and NotI sites. COS7 and 293T cells were cultured in DMEM supplemented with 10% (vol/vol) FBS (HyClone), penicillin, and streptomycin. COS7 cells stably expressing lunapark-mCherry were made by lentiviral transduction. Lentivirus was produced in 293T cells according to standard protocols and was used to infect COS7 cells. Cells were subsequently selected with blasticidin.

COS7 cells expressing lunapark mCherry were plated sparsely on acid-washed 18-mm glass coverslips and fixed and stained as previously described (12). Cells were fixed with 4% (vol/vol) paraformaldehyde, permeabilized with 0.1% Triton X-100. Immunostaining for calreticulin was performed using rabbit polyclonal antibody (Abcam) at 1 μg/mL and Alexa 488-conjugated secondary antibodies (Life Sciences) at 1 μg/mL in PBS containing 1% calf serum. Coverslips were mounted in Vectashield (Vector Labs). Images were acquired using a Yokogawa spinning-disk confocal on a Nikon TE2000U inverted microscope with a 60× Plan Apo N.A. 1.4 objective lens, and a Hamamatsu ORCA ER-cooled CCD camera. Images were analyzed with MetaMorph software in their original 12-bit format. mCherry signal was acquired directly and calculated by measuring average intensity in a cell and then subtracting a background average intensity value measured in uninfected COS7 cells. For presentation purposes, images were converted to 8-bit format and imported into Adobe Photoshop.

Superresolution Experiments. COS-7 cells (American Type Culture Collection) were cultured with DMEM (Invitrogen) containing 10% (vol/vol) FBS (Serum Source International), 100 IU/mL penicillin, and 0.1 mg/mL streptomycin, and incubated at 37 °C with 5% (vol/vol) CO_2. The cells were seeded into LabTek eight-well coverglass chambers at a density of 30,000 cells per well. The cells were fixed and stained 1 d after seeding. The fixation and immunostaining protocol consisted of the following: washing with fresh culture medium; fixation with 3% (vol/vol) paraformaldehyde (Electron Microscopy Sciences) and 0.1% glutaraldehyde (Electron Microscopy Sciences) in PBS; washing with PBS;

reduction with ~10 mM aqueous sodium borohydride for 7 min; washing with PBS; blocking and permeabilization with 3% (wt/vol) BSA (Jackson ImmunoResearch Laboratories) and 0.5% Triton X-100 (Sigma-Aldrich) in PBS for 45 min; staining for 45 min with goat anti-Nogo A primary antibody (Santa Cruz Biotechnology) at a concentration of 2 μg/mL in blocking buffer and a polyclonal rabbit anti-calreticulin primary antibody (Abcam) at a dilution of 1:100 in blocking buffer; washing with PBS; staining for 45 min with donkey anti-goat and donkey anti-rabbit secondary antibodies each bearing ~3 Alexa 647 or ~3 Cy3B fluorophores per antibody and at concentrations of ~2.5 μg/mL in blocking buffer (antibody labeling was performed as described previously) (13); washing with PBS; postfixation in a mixture of 3% (vol/vol) paraformaldehyde and 0.1% glutaraldehyde in PBS for 10 min; and washing with PBS. The initial wash and fixation steps were performed at 37 °C, and remaining steps were performed at ambient temperature (~21 °C).

STORM imaging was performed on a customized Olympus IX-71 inverted fluorescence microscope with a high numerical aperture oil immersion objective lens (100× UPlanSApo, 1.4 N.A.; Olympus) and a home-built near-infrared focus lock system previously described (13). The fluorescence signal was detected using an Andor iXon 897 electron-multiplying CCD camera at a frame rate of 60 Hz. The two-channel data were acquired sequentially using different imaging cubes for each of the two fluorophores. The Alexa 647 STORM image was acquired first, using 657-nm laser illumination (RCL-300-656; CrystaLaser) with a long-pass dichroic mirror (T660LPXR; Chroma) and a bandpass emission filter (ET705/72m; Chroma). The Cy3B STORM image was acquired second, using 561-nm laser illumination (Sapphire 561-200; Coherent) with a long-pass dichroic mirror (ZT561RDC; Chroma) and a bandpass emission filter (FF01-607/70-25; Semrock). Near-total internal reflection illumination was used with an intensity of 2–4 kW/cm^2 for the 657-nm and 561-nm laser lines (14). A 405-nm laser (CUBE 405-50C; Coherent) was used to activate dark-state fluorophores during acquisition and was ramped up from ~0–200 W/cm^2 during the course of the movie. Images of the cells were acquired in 0.2 M Tris, pH 8, 143 mM 2-mercaptoethanol, and an oxygen scavenging system [0.5 mg/mL glucose oxidase (Sigma-Aldrich), 40 μg/mL catalase (Sigma-Aldrich), and 10% (wt/vol) glucose]. STORM movies were analyzed using procedures similar to those previously described (15). The two-channel STORM images were manually registered, using a simple *x-y* translation of one of the channels relative to the other.

ER Network Formation in Crude *Xenopus* Extracts. Crude extracts from metaphase-arrested *X. laevis* eggs (CSF extract) were prepared as described (16). An aliquot of CSF extract was prelabeled with 100 μg/mL DiIC$_{18}$ (1,1′-dioctadecyl-3,3,3′,3′-tetramethylindocarbocyanine perchlorate; Invitrogen) for 45 min at 18 °C. ER network assembly reactions were prepared by adding 1:10 volume of prelabeled CSF extract to fresh extract, followed by addition of 0.4 mM CaCl$_2$ and 10-min incubation at 18 °C to release the metaphase arrest. An aliquot of the DiIC$_{18}$-labeled interphase extract (8 μL) was placed between two 22 × 22-mm PEG-pretreated glass coverslips. The samples were sealed and mounted over a metal slide with a 20-mm round hole using VALAP (1:1:1 mix of Vaseline, paraffin, and lanolin). Samples were incubated at 18 °C for 15 min before imaging, using a spinning-disk confocal fluorescence microscope. Mitotic ER networks were prepared in the same way, except that a DiIC$_{18}$-labeled interphase extract was supplemented with 50 μg/mL of cyclin BΔ90 to induce mitosis (17).

The samples were visualized with a Yokogawa CSU-X1 spinning-disk confocal with Borealis modification (Spectral Applied Research) on a Nikon Ti inverted microscope equipped with 60× Plan Apo N.A. 1.4 oil immersion and 100× Plan Apo N.A. 1.45 objective lenses and the Perfect Focus System for continuous maintenance of focus. Green fluorescence images were collected using a 491-nm solid-state laser from an LMM-5 laser launch controlled with an AOTF (Spectral Applied Research) and ET525/50 emission filter (Chroma). Red fluorescence images were collected using a 561-nm solid-state laser-controlled with an AOTF (Spectral Applied Research) and ET620/60 emission filter (Chroma). All images were acquired with a Hamamatsu ORCA AG cooled CCD camera controlled with MetaMorph software (version 7.0; Molecular Devices) and archived using ImageJ. Linear adjustments were applied to enhance the contrast of images in ImageJ.

To quantitate the connectivity of ER tubules, a custom ImageJ script was used. Briefly, the script converted the image to a binary mask and used a skeleton function to obtain a single pixel-wide representation of the ER network. Each positive (x, y) pixel in this topological representation was analyzed with a custom-defined function. Pixels displaying two neighbor pixels with a positive value correspond to tubules, and pixels with three or four neighbor pixels displaying a positive value corresponded to three- or four-way junctions, respectively.

The 3D representations of three-way junctions were constructed using confocal slices of the ER network and the 3D visualization software bioView3D (18).

ER Network Formation with Isolated Membranes. The fractionation of *Xenopus* extracts and ER network formation from isolated membranes were performed, as described previously (16). Briefly, 0.5 μL of DiIC$_{18}$- or DiOC$_{18}$-prelabeled membranes were resuspended in 9 μL of ELB200 [50 mM Hepes-KOH (pH 7.5), 200 mM KCl, 2.5 mM MgCl$_2$, 250 mM sucrose] containing 1 mM DTT and protease inhibitors and a 20× energy regenerating system (2.5 mg/mL creatine phosphokinase, 250 mM phosphocreatine, 50 mM ATP, 10 mM GTP). An aliquot of the sample was placed into a no. 1.5 coverslip, passivated as described previously (16). The sample was sandwich-sealed with VALAP and incubated for 2 h at room temperature. Imaging was done as described for experiments with crude extracts.

1. Terasaki M, et al. (2013) Stacked endoplasmic reticulum sheets are connected by helicoidal membrane motifs. *Cell* 154(2):285–296.
2. Helfrich W (1973) Elastic properties of lipid bilayers: Theory and possible experiments. *Z Naturforsch C* 28(11):693–703.
3. Spivak M (1970) *A Comprehensive Introduction to Differential Geometry* (Publish or Perish, Houston).
4. Niggemann G, Kummrow M, Helfrich W (1995) The bending rigidity of phosphatidylcholine bilayers: Dependences on experimental method, sample cell sealing and temperature. *J Phys II France* 5(3):413–425.
5. Markin VS (1981) Lateral organization of membranes and cell shapes. *Biophys J* 36(1): 1–19.
6. Siegel DP, Kozlov MM (2004) The Gaussian curvature elastic modulus of N-monomethylated dioleoylphosphatidylethanolamine: Relevance to membrane fusion and lipid phase behavior. *Biophys J* 87(1):366–374.
7. Hu M, Briguglio JJ, Deserno M (2012) Determining the Gaussian curvature modulus of lipid membranes in simulations. *Biophys J* 102(6):1403–1410.
8. Zilman A, Tlusty T, Safran SA (2002) Entropic networks in colloidal, polymeric and amphiphilic systems. *J Phys Condens Matter* 15:S57–S64.
9. Tlusty T, Safran SA (2000) Microemulsion networks: The onset of bicontinuity. *J Phys Condens Matter* 12:A253–A262.
10. Hu J, et al. (2008) Membrane proteins of the endoplasmic reticulum induce high-curvature tubules. *Science* 319(5867):1247–1250.
11. Brakke KA (1992) The surface evolver. *Expo Math* 1:141–165.
12. Shibata Y, et al. (2008) The reticulon and DP1/Yop1p proteins form immobile oligomers in the tubular endoplasmic reticulum. *J Biol Chem* 283(27):18892–18904.
13. Vaughan JC, Dempsey GT, Sun E, Zhuang X (2013) Phosphine quenching of cyanine dyes as a versatile tool for fluorescence microscopy. *J Am Chem Soc* 135(4):1197–1200.
14. Konopka CA, Bednarek SY (2008) Variable-angle epifluorescence microscopy: A new way to look at protein dynamics in the plant cell cortex. *Plant J* 53(1):186–196.
15. Huang B, Wang W, Bates M, Zhuang X (2008) Three-dimensional super-resolution imaging by stochastic optical reconstruction microscopy. *Science* 319(5864): 810–813.

16. Wang S, Romano FB, Field CM, Mitchison TJ, Rapoport TA (2013) Multiple mechanisms determine ER network morphology during the cell cycle in X*en*opus egg extracts. *J Cell Biol* 203(5):801–814.
17. Murray AW, Solomon MJ, Kirschner MW (1989) The role of cyclin synthesis and degradation in the control of maturation promoting factor activity. *Nature* 339(6222): 280–286.
18. Kvilekval K, Fedorov D, Obara B, Singh A, Manjunath BS (2010) Bisque: A platform for bioimage analysis and management. *Bioinformatics* 26(4):544–552.

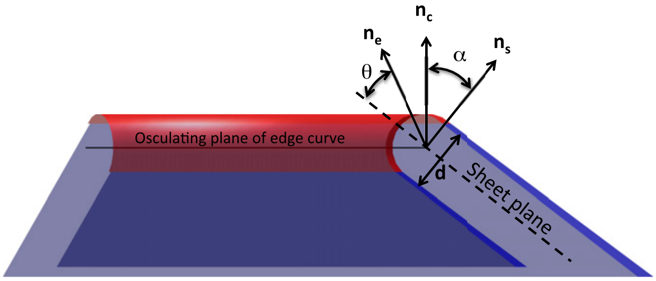

Fig. S1. Geometric properties used in the theoretical model. The scheme shows the angle α between a normal to the osculating plane of the edge line, $\boldsymbol{n_c}$, and a normal to the sheet plane, $\boldsymbol{n_s}$. Also shown is the angle θ between a normal to a point on the edge surface, $\boldsymbol{n_e}$, and the sheet plane.

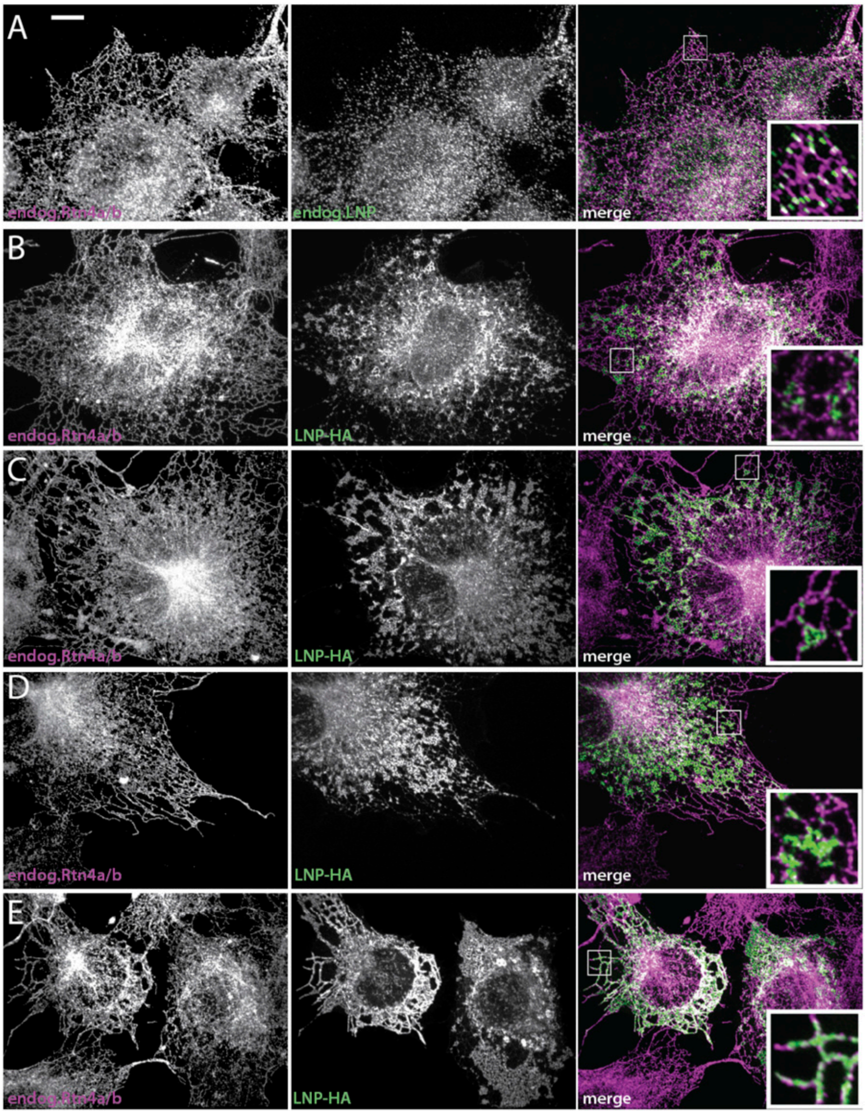

Fig. S2. Localization of lunapark protein and reticulon 4a/b in COS cells. (*A*) The localization of Lnp and Rtn4a/b was determined by immunostaining using specific antibodies. The samples were analyzed by confocal microscopy. (*Right*) Merged image. (*B*) An HA-tagged version of lunapark (Lnp-HA) was transiently expressed in COS cells and its localization compared with that of endogenous Rtn4a/b. The samples were analyzed by fluorescence microscopy using HA and Rtn4a/b antibodies. Shown is a cell that expresses Lnp-HA at a low level. (*C–E*) As in *B*, but with progressively higher expression levels of Lnp-HA. (Scale bar: 10 μm.)

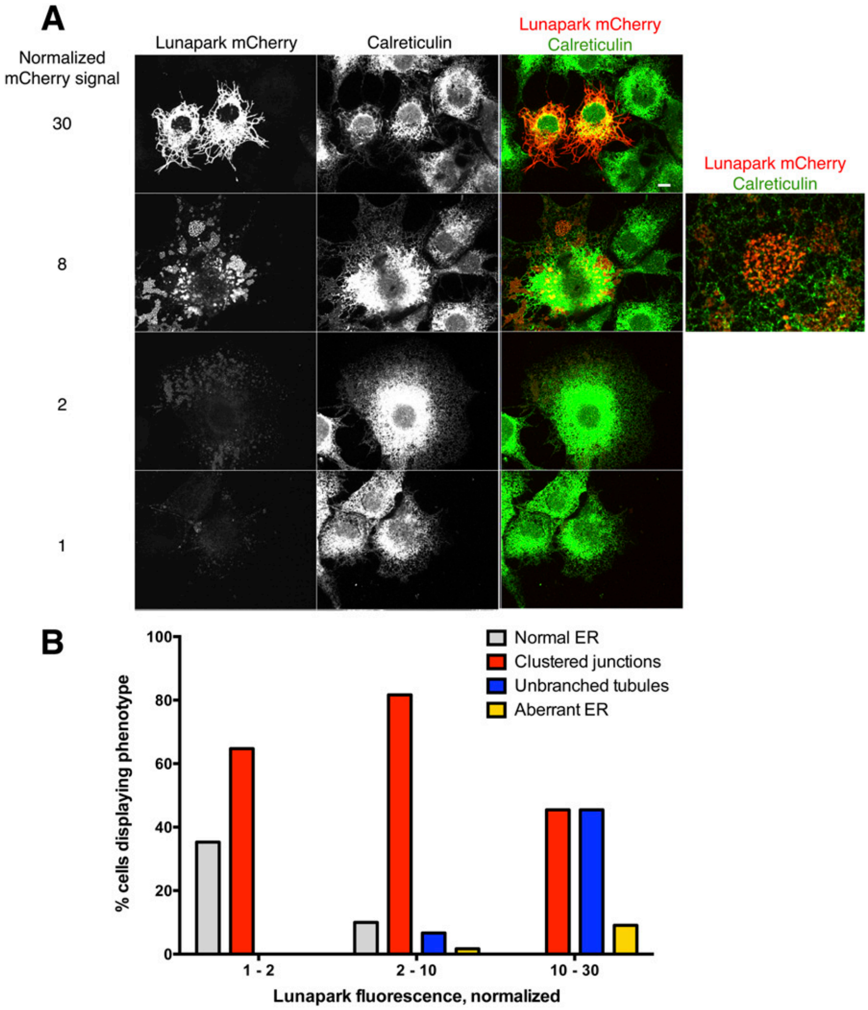

Fig. S3. Stable expression of lunapark in COS7 cells. (*A*) COS7 cells stably expressing mCherry-tagged lunapark were immunostained for endogenous calreticulin, displayed in grayscale or green. mCherry signal was visualized directly, displayed in grayscale or red. Each row corresponds to a different level of lunapark overexpression, ordered from high to low. mCherry levels are expressed and compared using arbitrary units of fluorescence signal. (Scale bar: 10 μm.) (*B*) Images of individual cells acquired as described in *A* were scored for ER phenotypes; they were then analyzed for mCherry fluorescence level and binned into low, medium, and high expression-level groups, as indicated on the *x* axis. The percentage of each phenotype in a given expression level bin is shown.

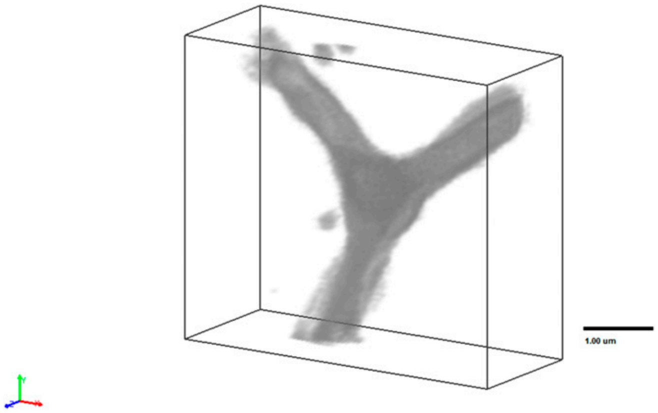

Movie S1. A 3D reconstruction of a dilated three-way junction. Video of a 3D reconstruction of a three-way junction between dilated ER tubules formed with *Xenopus* egg membranes. An ER network was formed and imaged as described in Fig. 3*B*. Images from successive confocal planes were combined to reconstruct the structure. (Scale bar: 1.55 μm.)

Movie S1